Published in final edited form as:
NMR Biomed. 2014 August ; 27(8): 939–947. doi:10.1002/nbm.3139.

Metabolic spectroscopy of inflammation in a bleomycin-induced lung injury model using hyperpolarized 1-^{13}C pyruvate

Hoora Shaghaghi[*,a], **Stephen Kadlecek**[a], **Charuhas Deshpande**[b], **Sarmad Siddiqui**[a], **Daniel Martinez**[c], **Mehrdad Pourfathi**[a], **Hooman Hamedani**[a], **Masaru Ishii**[d], **Harrilla Profka**[a], and **and Rahim Rizi**[a]

[a] Department of Radiology, University of Pennsylvania, Philadelphia, PA, United States

[b] Department of Pathology and Laboratory Medicine, University of Pennsylvania, Philadelphia, PA, United States

[c] Department of Pathology and Pathology Core Laboratory, Children's Hospital of Philadelphia, Philadelphia, PA, United States

[d] Department of Otolaryngology, Johns Hopkins University, Baltimore, MD, United States

Abstract

Metabolic activity in the lung is known to change in response to external insults, inflammation, and in cancer. We report measurements of metabolism in the isolated, perfused rat lung of healthy controls and in diseased lungs undergoing acute inflammation using hyperpolarized 1-^{13}C-labeled pyruvate. The overall apparent activity of lactate dehydrogenase is shown to increase significantly (on average by a factor of 3.3) at the 7-day acute stage and to revert substantially to baseline at 21 days, while other markers indicating monocarboxylate uptake and transamination rate are unchanged. Elevated lung lactate signal levels correlate well with phosphodiester levels as determined with ^{31}P spectroscopy and to the presence of neutrophils as determined by histology, consistent with a relationship between intracellular lactate pool labeling and the density and type of inflammatory cells present. We discuss several alternate hypotheses, and conclude that the most probable source of the observed signal increase is direct uptake and metabolism of pyruvate by inflammatory cells and primarily neutrophils. This signal is seen in high contrast to the low baseline activity of the lung.

Keywords

Lung; Inflammation; Hyperpolarized; Metabolism; Neutrophil; Macrophage

Introduction

The metabolic state of the lung is known to change rapidly in response to insult, and is particularly responsive to injury during overdistention and exposure to particulates or other

[*]Author to whom correspondence should be addressed: hoorash@mail.med.upenn.edu Submitting author: Hoora Shaghaghi, PhD University of Pennsylvania Department of Radiology 338 Stemmler Hall 3450 Hamilton Walk Philadelphia, PA 19104 215-662-6775 hoorash@mail.med.upenn.edu.

hazardous compounds (1,2). Although some debate remains with respect to the role and side-effects of lung infiltration by inflammatory cells, it is generally accepted that inflammatory cell activity, and particularly that of neutrophils (3), can exacerbate ischemia-reperfusion injury and ventilator-induced lung injury. A similar mechanism may be responsible for the onset of Acute Respiratory Distress Syndrome (ARDS) and the release of matrix metalloproteases linked to the progression of emphysema. There is now convincing evidence that inappropriate or excessive pulmonary inflammatory response contributes to a variety of lung disorders, and that techniques for reducing neutrophil infiltration may lead to better clinical outcomes (4,5).

Accordingly, it would be useful to visualize and quantify the progression of lung inflammation to directly inform a wide variety of clinical decisions, for instance in gauging the inflammatory response in ARDS or during a COPD (Chronic Obstructive Pulmonary Disease) exacerbation. Unfortunately, direct imaging of inflammatory cell infiltration or activity is difficult. In disease models, neutrophil and macrophage counting in biopsy samples and lavage fluid is commonly performed, but the techniques do not reflect the well-known regional heterogeneity of inflammation and are undesirable in clinical care. X-ray / CT imaging is also not well suited to this application, as x-ray absorption depends much more strongly on edema, fibrosis, emphysema, and other alterations to tissue density than on the weak direct x-ray absorption of the inflammatory cells. The one technique which has shown promise for visualizing inflammatory cell activity is ^{18}FDG-PET (3,5-9). The radiolabeled glucose analog, most commonly used for highlighting the elevated glycolytic activity of tumors, has been shown to be rapidly taken up by neutrophils due to their dependence on glycolysis for energy (10-12). However, the use of PET in follow-up or screening applications is inadvisable due to the associated radiation exposure.

On the other hand, hyperpolarized (HP) MRI is an emerging medical technology that enhances the polarization of a nucleus up to 10000-fold from its intrinsic thermal polarization. Many organic molecules, such as pyruvate, can be labelled with carbon-13 (non-zero spin) and polarized using commercially available hardware. As a result, HP MRI can be potentially used to detect metabolites at micromolar concentrations. If similarly sensitive to ^{18}FDG-PET, hyperpolarized 1-^{13}C pyruvate would provide a safe, viable alternative to FDG-PET for use as a marker for inflammation.

In this study, we address the hypothesis that uptake and metabolism of hyperpolarized 1-^{13}C pyruvate by inflammatory cells is rapid and displays sufficient additional signal to be easily distinguished from metabolism by the healthy lung tissue. We have used intratracheal instillation of bleomycin since this is a well-established model of acute pulmonary inflammation (13).

Materials and Methods

All animal experiments were conducted in accordance with protocols approved by the Institutional Animal Care and Use Committee of the University of Pennsylvania. 8-week-old male Sprague-Dawley rats weighing 320 +/− 20 g were used for all experiments. All rats were carefully age matched and maintained under very similar environments and dietary

conditions. Seven healthy control rats and thirteen bleomycin-exposed rats were used in the study.

Bleomycin Model Induction

Bleomycin model animals were anesthetized using inhaled 2.5% isoflurane, were placed supine, and were intubated with a 2-inch-long, 14-gauge angiocatheter. A 2.5 U/kg concentration of bleomycin (Bedford Laboratories, Bedford, OH) was then instilled through the catheter, followed by a 3-mL injection of air to clear the catheter. Animals were then rocked from side to side to distribute the bleomycin throughout the lungs as evenly as possible. The animals were subsequently recovered from anesthesia and briefly ventilated with a rodent ventilator (CWE Inc, Ardmore, PA) and supplemental oxygen was given if they failed to recover from anesthesia in a timely manner. Of the thirteen bleomycin-exposed animals, ten were imaged at 7 or 8 days post-induction and three at 21-days post-induction. All successfully underwent the MRI procedures. One of the 7-day hyperpolarized spectroscopy experiments failed for technical reasons, and one of the ^{31}P spectra was rejected because transient noise problems made it impossible to analyze.

Preparation of Lungs for Spectroscopy

The subjects were anesthetized with i.p. pentobarbital, tracheostomy was performed, and 200 U heparin was administered via tail vein. The lungs were prepared for the NMR study according to the previously reported method of “degassing” (14,15). That is, the animals were ventilated with pure O_2 (50 bpm, 11-14 cm H_2O PIP) for 10 minutes in order to remove all N_2 from the airways. After ventilation, the trachea was sealed (end exhalation) with a suture, allowing residual O_2 to be absorbed by the circulating blood and perfusate. Thoracotomy was immediately started, the heart was cut transversely, and the pulmonary artery was cannulated via the right ventricle. After perfusion was started, the lungs were rapidly excised and placed in a 20-mm NMR tube. The lungs were perfused at 10 mL/min with a modified Krebs-Henseleit buffer: 119 mM NaCl, 25 mM $NaHCO_3$, 1.3 mM $CaCl_2$, 1.2 mM $MgSO_4$, 4.7 mM KCl, 10 mM glucose, 3% (w/v) fatty acid free bovine serum albumin (BSA, Fisher Bioreagents). The perfusate was passed through an oxygenating column under a constant flow of 1 atm 95:5 O_2/CO_2, and warmed via passage through water-jacketed tubing. The CO_2 concentration in the oxygenating column was chosen to maintain constant perfusate pH during oxygenation, although periodic adjustment with 1M HCl or NaOH was needed to maintain a physiological value of 7.4 ± 0.1. The lung was submerged in perfusate throughout the experiment. The temperature of the perfusate in the NMR tube was continuously monitored and maintained at 36.5 ± 1 C.

Preparation and administration of hyperpolarized 1-^{13}C pyruvate

28.5 mg [1-^{13}C]pyruvic acid (Cambridge Isotope Laboratories) mixed with 15 mM OX063 trityl radical (Oxford Instruments) and 1.5 mM Dotarem Gd chelate (Guerbet) was polarized to ~30% at 1.42 K and 94 GHz with a HyperSense DNP system (Oxford Instruments). 4 mL of buffer, containing 50mM Tris, 80mM NaOH, and 100 mg/L EDTA, was heated to 190°C at 10 bar, and was used to rapidly dissolve the frozen sample. This sample was further diluted in 6.0 mL oxygenated Krebs-Henseleit buffer (without BSA, which was found to cause unacceptable signal loss during sample transport), yielding a neutral, isotonic solution

of 32 mM [1-^{13}C] pyruvate. This solution was injected into the perfusate line at 10 mL/min in lieu of the steady-state perfusion buffer. After the 60 seconds required to inject the hyperpolarized solution, lung perfusion was restored.

Magnetic Resonance Spectroscopy

All MR spectra and images were obtained using a 9.4T vertical bore magnet (Varian, Inc., Palo Alto, CA) equipped with a gradient insert (Resonance Research, Inc., Billerica, MA) and a 20mm ^{1}H/broadband probe (Doty Scientific, Columbia, SC). After insertion into the bore of the magnet, the sample was tuned, matched and shimmed to a linewidth of about 40 Hz. This required approximately 20 minutes. Immediately following, the lung was ^{1}H-imaged (10 2-mm axial slices, field of view FOV = 30×30 mm) for positioning and to ensure the integrity of the organ and the absence of edema. Next, a whole-lung, averaged ^{31}P spectrum was acquired to assess the energy status of the lung (repetition time TR = 1s, nominal flip-angle $\alpha = 60°$, acquisition time AT = 200 ms, spectral width SW = 100 kHz, 512 averages). The probe was then tuned to ^{13}C and the perfusate was temporarily replaced by the hyperpolarized solution. Low flip-angle spectra were acquired for the several-minute duration of the hyperpolarized signal (TR = 1s, nominal $\alpha = 10°$, AT = 800 ms, SW = 20 kHz, 300 individual spectra acquired). Following the ^{13}C spectroscopy, another averaged ^{31}P spectrum was acquired in order to evaluate changes in ATP status due to the hyperpolarized compound injection. In seven instances, the entire series was then repeated (^{31}P spectrum, hyperpolarized spectrum series, ^{31}P spectrum) after a one hour delay required to hyperpolarize another pyruvate sample. This was done to evaluate the stability and reproducibility of the lung and its metabolic activity.

Quantitative evaluation of NMR spectra

^{31}P spectra were least-squares fit to 13 Lorentzian peaks allowing the individual peak heights and common peak width to vary freely. The peak frequencies were kept fixed; peak identities and ppm chemical shifts relative to PCr (see **Figure 1** caption for acronyms) were: PME (6.70), Pi (5.08, 4.32), GPC (3.03), GPE (2.24), PG (1.80), PCr (0.00), γ-NTP (-2.36), α-NTP (-7.52), DPDE/NAD(H) (-8.18, -9.68, -11.49, -13.30), and β-NTP (-16.13). The quality of the fit was found to improve substantially by including three additional peaks of fixed position (3.5, -4 and -10 ppm) and width (3, 8 and 4 ppm, respectively) to account for contributions from unresolved ^{31}P species. We note that the region containing GPC, GPE and PG is poorly resolved and likely contains other phosphodiesters as well. Although consistent with previous measurements (16-17) the number and identity of resonances is uncertain.

^{13}C spectra were least-squares fit to 5 Lorentzian peaks allowing the individual peak heights to vary. The peak positions and widths were set using an initial free fit (amplitude, width and position) to the average of all spectra with S/N > 30. The peaks were identified as pyruvate, alanine, pyruvate hydrate, lactate and bicarbonate with ppm chemical shifts relative to pyruvate of 0.00, 5.68, 8.42, 12.26 and -9.98, respectively. Additional peaks representing natural abundance nuclei or impurities were not included in the fit. All peak fitting was done using custom software written in MATLAB (Natick, MA).

Histological evaluation

Immediately after the final MRS acquisition, nine of the lungs (3 each of control, 7-day and 21-day inflammation) were prepared for histological evaluation. The steady-state perfusion buffer was replaced by a 10% formalin solution and perfusion was continued for one minute, after which the lungs were submerged in 10% formalin for 5-7 days and subsequently embedded in paraffin. The lungs were not inflated prior to fixation due to the uncertainty of their response to re-inflation. Although inflating the lungs would have made the gross structure easier to visualize, we do not expect that it would have affected the ability to count the cells of interest. 25 transverse 5 μm sections were cut from each lung (5 groups of 5 contiguous sections spaced by 2 mm). Previous studies have indicated that neutrophils and macrophages represent the bulk of the inflammatory response to bleomycin-induced injury in rats (18, 19). As such, sections from each group were stained with Hematoxylin and Eosin (H&E), and with Anti-Neutrophil Elastase antibody (ab21595, abcam, Cambridge, MA) or CD68 antibody (SPM130, Santa Cruz Biotechnology, Dallas, TX), which have previously shown reactivity to rat neutrophil and macrophage, respectively. Because of significant non-specific binding, only the H&E sections were used to evaluate the extent of neutrophil and macrophage infiltration. An experienced lung pathologist blindly examined the 5 whole lung sections from each sample and assigned a grade from 0-4 with respect to neutrophils, macrophages, lymphocytes, and organizing pneumonia (OP) foci, based on the number of cells or sites present. No distinction was made among lymphocyte types. For each cell type, lungs with minimal cell density were assigned a grade of 0, whereas lungs with severe and widely distributed inflammatory cells were assigned a grade of 4. The grading scale was relative for each type of cell. For example, a section that scored a grade of 4 for both neutrophils and macrophages had a much greater number of neutrophils than macrophages. Each lung was then assigned a score for each cell type equal to the average rating among the sections.

Statistical methods

In order to test whether the three model groups were characterized by different means when measured using ^{13}C spectroscopy, ANOVA followed by Tukey's HSD post hoc was performed in the sixteen first measurements across the control, 7-day and 21-day bleomycin groups. Repeated measures ANOVA was performed in the subset of six lungs for which ^{13}C spectroscopy was repeated and the eighteen lungs in which repeated ^{31}P spectroscopy was performed to determine whether there was any evidence that the two measurements performed in the same lung were systematically different, In order to determine the extent of direct relationships between inflammation as measured using ^{13}C and ^{31}P spectroscopy, and between ^{13}C spectroscopy and inflammatory cell counts, simple correlations were calculated across all measurements in which both metrics were available. All statistical analyses were performed using the R software. R is an open-source project that is distributed under the GNU General Public License (Copyright 2007 Free Software Foundation, Inc.)

Results

^{13}C spectroscopy

Figure 1 displays a representative series of individual spectra from an inflamed lung. As with all such series, peaks corresponding to 1-^{13}C pyruvate and 1-^{13}C pyruvate-hydrate appeared first, followed within a few seconds by 1-^{13}C lactate, and 1-^{13}C alanine. All peaks were clearly distinguishable and quantifiable for a period of approximately two minutes after the first appearance of hyperpolarized signal. Additional peaks corresponding to natural abundance ^{13}C, impurities and ^{13}C-bicarbonate were smaller but also reliably quantifiable. Observed linewidths were typically ~15 Hz, which somewhat exceeded the expected ~40 Hz × γ_{13C} / γ_{1H} expected based on the ^{1}H shim. In the **Figure 1** inset, we overlaid spectra acquired 20-30 seconds after the end of the hyperpolarized injection in control, 7-day, and 21-day inflammatory model animals. As is typical of the comparison, pyruvate, pyruvate-hydrate and alanine signal levels were very similar, but the integrated lactate signal of the inflammatory model exceeded that of the control animal by approximately a factor of three. **Figure 2** displays the result of fits to each spectrum of the time-series in each subject. Although the observed lactate signal is more variable among the inflammatory model cohort, each of the 7-day inflammatory model lungs exhibited a greater observed lactate signal at all times than any of the control lungs; integrated lactate signals in the 7-day inflammatory group exceeded those of the control group by a factor of 3.1 on average (if repeated measurements in the same lung are excluded from the analysis, the 7-day group's signals are higher by an average factor of 3.3). Lactate signal levels in the 21-day cohort were midway between the control and 7-day groups, exceeding the control group by a factor of 1.8 on average. Means and standard deviations of all three groups are summarized in the **Figure 2** inset.

^{31}P spectroscopy

Figure 3 shows two averaged ^{31}P spectra, representative of the normal (green) and 7-day inflammatory (red) lung cohorts. Eight distinct ^{31}P-containing species can be discerned (16-17,20-21); of these, only phosphoglycans and the phosphodiesters (primarily glycerophosphocholine and glycerophosphoethanolamine) differ significantly between the normal and inflamed lung, and are elevated by a factor of 2.5 in inflammation on average. Some inconsistency in the fit values arises from limited signal-to-noise in the ^{31}P spectra. Some inconsistency in the position and width of the inorganic phosphate peak is seen as well, which may indicate variability in tissue pH despite the narrow range of perfusate pH.

Histology

Representative H&E sections from the control, 7-day and 21-day inflammatory cohorts appear in **Figure 4**. These sections were chosen to highlight the visually apparent trend of dramatically elevated neutrophils at day 7, which were partially resolved by day 21, and of progressively increasing macrophage count from day 7 to day 21. This trend can be seen more clearly in the inflammatory cell scores from each lung (**Table 1**). On average, the neutrophil scores at 7 and 21 days exceeded the control scores by factors of 3.8 and 2.6, respectively, and the inflammatory macrophage scores exceeded the control scores by factors of 3.9 and 6.6, respectively. There are some transient OP foci present in day 7

sections, but most of these foci are resolved by day 21. The 21-day sections have minimal OP foci, but were characterized by protein deposits (Figure 4) that can signify fibrotic remodeling, and which was only minimally apparent at 7 days. Notably, the 21-day cohort contained one subject which was visually similar to the 7-day cohort, with respect to both active neutrophilic inflammation and relative lack of fibrosis. This subject also exhibited ^{31}C and ^{31}P spectroscopy results which were elevated with respect to control and the other 21-day lungs, and which were consistent with the 7-day cohort (figures 2 and 3).

Statistical tests

Application of ANOVA among the sixteen first ^{13}C measurements revealed that the three experimental groups are characterized by significantly different means ($F(2,13) = 15.9$, $p = 0.0004$). Further analysis using the Tukey HSD test was performed to determine whether significance exists between the cohorts. The results are presented in **Table 2**. The mean lactate labeling of the day 7 bleomycin group was significantly higher than either of the two other groups; on the other hand, we could not show a significant difference between the day 21 bleomycin and the control group. Although with less significance, the ^{31}P spectroscopy data yielded identical results in post hoc analysis.

Application of repeated measures ANOVA among the six repeated ^{13}C spectroscopy measurements in the two groups (two controls, four day 7 bleomycin) showed that there was a significant difference between the means of the two groups ($F(1,4) = 193.4$, $p=0.0002$), and the hypothesis that the repeated ^{13}C measurements are characterized by the same mean within experimental repeats was not rejected ($p = 0.88$). Similarly, the application of repeated measures ANOVA among the eighteen repeated ^{31}P spectroscopy tests in three groups (six control, ten 7-day bleomycin, two 21-day bleomycin) shows that there is a significant difference among the means of the three groups ($F(1,4) = 4.27$, $p = 0.036$). Similar to the ^{13}C data, there was no difference in the repeated experimental measurements within groups ($p = 0.26$). There is no statistical evidence for any interaction between the experimental group and measurement number ($p = 0.84$ and 0.16 for ^{13}C and ^{31}P spectra, respectively).

Figure 5 summarizes the relationship between elevated GPC/E levels and elevated lactate production within and between study groups. Across all study animals, a significant correlation was found ($r = 0.69$ / 0.74 if all / first injections are analyzed ($p < 0.001$ in both cases).

Figure 6 shows the correlation between the measured lactate signal and the histologically-determined neutrophil and macrophage scores for the eight subjects for which both measures were available. The correlation coefficient is statistically significant ($r = 0.89$, $p < 0.005$) when lactate signal and neutrophil score are compared but is not significant ($r = 0.36$, $p = 0.39$) when lactate signal and macrophage score are compared.

Discussion

The main finding of this work is that a common experimental model of lung inflammation affects the metabolic activity of the lung such that the overall apparent lactate

dehydrogenase (LDH) activity is increased substantially 7 days post-induction. Activity returns substantially to baseline 21 days post-induction, although the smaller sample size in the latter group does not allow unambiguous determination that activity remains somewhat elevated. We believe that the increase at 7 days is indicative of direct uptake and metabolism of pyruvate by inflammatory cells, primarily neutrophils, which have infiltrated the lung in response to the bleomycin insult.

Several other explanations are possible, which we will discuss individually. First, it is known that other conditions may affect apparent LDH activity. In a previous study (22), we showed that temporary hypoxia can increase lactate labeling in the perfused lung by a similar factor to that observed here, most likely due to the increased intracellular lactate pool size and consequent increase in NAD+ reduction rate. While it is possible that damage to the lung (e.g., fibrosis or emphysema-like tissue degradation) may adversely affect gas transport and tissue oxygenation, the primary means of oxygenation in this study is via the oxygenated perfusate. Any tissue damage that prevents adequate contact with the perfusate would also hinder access to the hyperpolarized agent, delivered through the same flow path, making hyperpolarized lactate signals in those regions unobtainable. Furthermore, the hypoxic lung exhibited a distinctively low PCr and NTP signal in ^{31}P spectroscopy when studied previously (22). These distinctive changes were not observed in this study.

Another possible cause of increased lactate signal is a change in the uptake of pyruvate by the lung tissue. Although transporter activity may be affected by energy status, pH and other factors of the extra- and intracellular environment (23), no alteration in transport was detected in the inflammatory model lungs. We note that hyperpolarized alanine signal is not significantly increased in the inflammatory model animals; if pyruvate uptake by pneumocytes were increased sufficiently to explain the increased lactate signal, we would expect a measurably increased rate of transamination in these cells as well. It is possible that pyruvate uptake and transamination were both significantly and inversely altered such that the transfer of label to the alanine pool remained unchanged, but we would consider this an unlikely coincidence.

Third, it is possible that the increased apparent LDH activity observed arises in part from extracellular LDH. Although intracellular in healthy tissue, LDH is known to be present in substantial concentration in the extracellular space in regions experiencing cell death; tests of bronchoaveolar lavage fluid LDH activity are a common nonspecific indicator of tissue damage (24,25). In this case, however, the persistence of the lactate signal (along with pyruvate and alanine, but in contrast to pyruvate hydrate) is a clear indication of its intracellular origin; if it were extracellular, it would be washed out rapidly once ordinary perfusion is restored, as is the case for the extracellular pyruvate-hydrate and other impurities (**Figure 1**). The continued linear increase of the lactate:pyruvate ratio during this washout period is most likely indicative of the intracellular rate constant for forward LDH activity, although it may also reflect the efflux of pyruvate from the lung epithelium. This process has been shown to be rapid and dynamic (26).

A final possible cause of increased lactate signal in the inflammatory model lungs is the change in redox status of the lung tissue due to reactive oxygen species originating from the

respiratory burst phase of neutrophil activity. These compounds may interact directly with the NADH/NAD^+ redox couple, indirectly through modulation of glutathione-mediated inhibition of LDH (27), or through a variety of other inflammatory signaling pathways (28).

Although this possibility cannot be ruled out based on the studies described here, it seems more likely that the increased lactate production arises from the rapid glycolysis of inflammatory cells. With respect to the similarly increased ^{18}FDG-PET signal in inflammation, autoradiographic studies (6,29,30) have confirmed that the source of the increase is primarily neutrophilic uptake, rather than an inflammatory-mediated change in lung tissue activity, and that the dramatically greater glycolytic rate of neutrophils (11) is sufficient to overwhelm signal originating in the lung epithelium. Given that the neutrophil glycolytic rate is not limited by LDH activity (31), we expect that similar dynamics are responsible for the substantial increase in lactate signal observed here.

It is possible that the increased macrophage density is responsible for some of the signal as well. However, the results of **Figure 6** provide evidence that the increased lactate labeling is primarily neutrophilic in origin. As seen in **Table 1** (and described previously (18)), neutrophil count in the bleomycin rat model peaks at approximately 7 days and is substantially returned to baseline 21 days after insult. In contrast, macrophage count continues to rise, peaking between 14 and 21 days. The neutrophil count time course is in qualitative agreement with the observed lactate signal time course (which is significantly higher at 7 days than at 21 days), and this agreement is reflected in the significance of the corresponding correlation plot of **Figure 6**.

The degree of lactate increase is fairly consistent with estimates of cell populations and metabolic characteristics available from previous studies. Pyruvate uptake and transformation to lactate in the normal lung is likely dominated by type II pneumocytes (32), given their rapid and highly glycolytic metabolism (32), large population (~5.5×10^7 cells per lung, double that of type I pneumocytes and ~6 times that of alveolar macrophages (33)), and conclusions based on cell morphology and oxygen uptake experiments (34). Assuming that the lavage cell counts are representative of inflammatory cell sub-populations, which has been demonstrated previously (35), bleomycin model lavage results suggest that the total inflammatory cell population increases by approximately a factor of 6 at 7 days and a factor of 3 at 21 days with respect to baseline (fig. 6 of 18,36-38), and that this increase consists almost exclusively of neutrophilic and macrophagic components (36-37). Previous studies have also shown that the type II pneumocyte population is slightly but not substantially diminished in this model (39-41). Although the degree and type of inflammatory cell activation is not known, we may approximate the expected relative contribution to hyperpolarized lactate signal by measured lactate production rates in cell culture; published results show that per cell lactate production of isolated alveolar macrophages (61 nmol/hr/10^6) and neutrophils (53 nmol/hr/10^6) are approximately equal, and exceed that of type II pneumocytes by approximately a factor of three (17 nmol/hr/10^6 cells (42-44)). Thus, these general considerations suggest that we should expect hyperpolarized lactate produced in the 7-day and 21-day bleomycin lungs to exceed that of the control lungs by factors of approximately 2.7 and 1.7, respectively. These values are comparable to the observed

factors of 3.1 and 1.8, and demonstrate that the proffered explanation is at least plausible given what is known about cell populations and metabolic activity.

The correlation between GPC/E levels as derived from ^{31}P NMR and lactate signal is another indication that hyperpolarized lactate imaging provides information about the extent and location of lung inflammation. It has been previously demonstrated that granulocytes contain very high levels of the phosphodiesters GPC and GPE (45), PG (46) and related (and spectroscopically indistinguishable) compounds. We therefore believe that the GPC/E levels of **Figure 3** are indicative of elevated inflammatory cell count characteristic of inflammation, and that the strong correlation with lactate signal seen in **Figure 5** provides evidence that both spectroscopic techniques are further elevated in more severe inflammation.

However, PET studies have also pointed out the need to interpret the signal increase carefully; it has been shown that the period of most rapid neutrophil energy metabolism does not correspond to the respiratory burst phase (47), but rather to cell migration and polarization. Because the former phase of neutrophil activity and the associated release of reactive oxygen species is likely responsible for the lung tissue damage associated with inflammatory exacerbations (48,49), it is possible that the period of maximum deleterious effect on the lung is not as conspicuous as the initial phase of neutrophil invasion when using either this technique or ^{18}FDG-PET.

A secondary finding of this study is that no systematic difference is observed between repeated measurements of inflammation in the same model lung using either ^{13}C or ^{31}P spectroscopy. Although the number of repeated ^{13}C spectroscopy measurements was limited, it is clear that the effect of repeated or delayed measurement on the lung is much smaller than the between-group differences. This serves as an indicator of model stability during perfusion, and suggests that small variations in timing do not affect the results of the experiment.

This study was limited to two time-points (7 and 21 days), and further investigation and comparison to histological markers will be required to relate this finding to more established measures of lung inflammation. In particular, we emphasize the highly dynamic nature (38) of cell counts and metabolic rates during acute inflammation; alveolar macrophages and neutrophils are known to undergo a greatly increased glycolytic rate during phagocytosis or when exposed to even the lowered O_2 tension of the healthy lung (50). Thus, the quantitative estimate of expected metabolic activity in inflammation is intended only as a plausibility argument based on cell populations, rather than as direct evidence for the source of the observed signal.

Furthermore, although the perfused lung model chosen has been shown to recapitulate many metabolic features of the *in situ* lung (51), the utility of this technique to localize and grade lung inflammation relies in part on a low baseline activity of the healthy tissue. The lung has previously been demonstrated to play a substantial role in the maintenance of glycolytic intermediate balance in the blood, which suggests that pyruvate and lactate transport and interconversion in the healthy organ may depend on whole-body metabolic activity,

dynamical perfusion effects, feeding and exercise status. Regions of the lungs may also express high apparent LDH activity during several other patholgoies, including cancer (52), environmental exposure to agents causing oxidative stress (53), or interstitial inflammation.

It is important to note that while the metabolic process examined here is related to the uptake and sequestration of ^{18}FDG, in that increased glycolytic activity can be expected to yield a larger signal, the two measurements are not equivalent. In particular, the imaging agents are transported into the cell via different mechanisms (GLUT1 vs, primarily, MCT2 (54)). The two enzymatic conversion processes are regulated through different means as well; most notably, hexokinase is inhibited by the FDG product FDG-6-phosphate and is the rate-limiting enzyme in neutrophilic glycolysis (31), while lactate dehydrogenase activity depends directly on cytosolic redox state and is regulated through a variety of other mechanisms including the inhibitory effect of the redox-coupled reduced glutathione concentration (27). Assessing the relative merits of each agent therefore requires further study in a model system.

Conclusions

We have demonstrated the use of non-ionizing, hyperpolarized ^{13}C spectroscopy and imaging to detect pulmonary inflammation and have provided evidence that the source of the observed signal is primarily infiltrating neutophils. Although dependent on different enzymatic and transport processes than those involved in ^{18}FDG imaging, many features of the techniques appear to be similar, including the several-fold increase of signal in inflammation and the apparent sensitivity to direct metabolism of the neutrophilic inflammatory component. Because the baseline metabolic activity of the lung epithelium is relatively low, neutrophilic activity is apparent in high contrast. The overall signal levels are raised such that imaging applications become feasible (55, 56), although the consistency of this low baseline and potential sensitivity to other conditions must be further investigated in both the isolated and *in situ* lung.

Acknowledgments

Sponsor: NIH Grant R01 EB010208

Abbreviations

AEII	Type II Alveolar Epithelial Cell
BSA	Bovine Serum Albumin
COPD	Chronic Obstructive Pulmonary Disease
CT	Computed Tomography
DNP	Dynamic Nuclear Polarization
DPDE	Diphosphodiester
EDTA	Ethylenediaminetetraacetic acid

FDG	Fluorodeoxyglucose
FOV	Field of view
GLUT1	Glucose Transporter 1
GPC	Glycerophosphocholine
GPE	Glycerophosphoethanolamine
LDH	Lactate Dehydrogenase
MCT2	Monocarboxylate Transporter 2PET- Positron Emission Tomography
NADH/NAD$^+$	Oxidized/reduced Nicotinamide adenine dinucleotide
NTP	Nucleoside 5'-triphosphate
PCr	Phosphocreatine
Pi	Inorganic phosphate
PME	Phosphomonoester

References

1. Mustafa MG, Cross CE. Effects of short-term ozone exposure on lung mitochondrial oxidative and energy metabolism. Arch. Biochem. Biophys. 1974; 1623(2):585–594. [PubMed: 4366422]
2. Magnani ND, Marchini T, Tasat DR, Alvarez S, Evelson PA. Lung oxidative metabolism after exposure to ambient particles. Biochem. Biophys. Res. Commun. 2011; 412(4):667–672. [PubMed: 21856280]
3. Locke LW, Williams MB, Fairchild KD, Zhong M, Kundu BK, Berr SS. FDG-PET quantification of lung inflammation with image-derived blood input function in mice. Int. J. Mol. Imag. 2011:1–6. doi:10.1155/2011/356730.
4. Ross SD, Tribble CG, Gaughen JR Jr, Shockey KS, Parrino PE, Kron IL. Reduced neutrophil infiltration protects against lung reperfusion injury after transplantation. Ann. Thorac. Surg. 1999; 67(5):1428–1433. [PubMed: 10355425]
5. Chen DL, Ferkol TW, Mintun MA, Pittman JE, Rosenbluth DB, Schuster DP. Quantifying pulmonary inflammation in cystic fibrosis with positron emission tomography. Am. J. Respir. Crit. Care Med. 2006; 173(12):1363–1369. [PubMed: 16543553]
6. Chen DL, Rosenbluth DB, Mintun MA, Schuster DP. FDG-PET imaging of pulmonary inflammation in healthy volunteers after airway instillation of endotoxin. J. Appl. Physiol. 2006; 100:1602–1609. [PubMed: 16424067]
7. de Prost N, Tucci MR, Vidal Melo MF. Assessment of Lung Inflammation with ^{18}F-FDG PET During Acute Lung Injury. Am. J. Roentgenol. 2010; 195(2):292–300. [PubMed: 20651183]
8. Bellani G, Messa C, Guerra L, Spagnolli E, Foti G, Patroniti N, Fumagalli R, Musch G, Fazio F, Pesenti A. Lungs of patients with acute respiratory distress syndrome show diffuse inflammation in normally aerated regions: a (^{18}F)-fluoro-2-deoxy-D-glucose PET/CT study. Crit. Care Med. 2009; 37(7):2216–2222. [PubMed: 19487931]
9. Jacene HA, Cohade C, Wahl RL. F-18 FDG PET/CT in acute respiratory distress syndrome: a case report. Clin. Nucl. Med. 2004; 29(12):786–788. [PubMed: 15545878]
10. McCall CE, Bass DA, Cousart S, DeChatelet LR. Enhancement of hexose uptake in human polymorphonuclear leukocytes by activated complement component C5a. Proc. Natl. Acad. Sci. USA. 1979; 76:5896–5900. [PubMed: 293691]
11. Borregaard N, Herlin T. Energy metabolism of human neutrophils during phagocytosis. J. Clin. Invest. 1982; 70:550–554. [PubMed: 7107894]

12. Jain V, Hasselquist S, Delaney MD. PET scanning in sarcoidosis. Ann. N. Y. Acad. Sci. 2011; 1228:46–58. [PubMed: 21718322]
13. Moeller A, Ask K, Warburton D, Gauldie J, Kolb M. The bleomycin animal model: a useful tool to investigate treatment options for idiopathic pulmonary fibrosis?. Int. J. Biochem. Cell. Biol. 2008; 40:362–382. [PubMed: 17936056]
14. Hayashi Y, Inubushi T, Nioka S, Forster RE. ^{31}P-NMR spectroscopy of isolated perfused rat lung. J. Appl. Physiol. 1993; 74(4):1549–1554. [PubMed: 8514668]
15. Pillai RP, Buescher PC, Pearse DB, Sylvester JT, Eichhorn GL. ^{31}P NMR spectroscopy of isolated perfused lungs. Magn Reson Med. 1986; 3(3):467–472. [PubMed: 3724427]
16. Kasimos JN, Merchant TE, Gierke LW, Glonek T. ^{31}P Magnetic resonance spectroscopy of human colon cancer. Cancer Res. 1990; 50:527–532. [PubMed: 2297695]
17. Pettegrew JW, Keshavan MS, Minshew NJ. ^{31}P Nuclear magnetic resonance spectroscopy: neurodevelopment and schizophrenia. Schizophr. Bull. 1993; 19(1):35–53. [PubMed: 8451612]
18. Otsuka M, Takahashi H, Shiratori M, Chiba H, Abe S. Reduction of bleomycin induced lung fibrosis by candesartan cilexetil, an angiotensin II type 1 receptor antagonist. Thorax. 2004; 59:31–38. [PubMed: 14694243]
19. Xx301. Chandler DB, Hyde DM, Giri SN. Morphometric estimates of infiltrative cellular changes during the development of bleomycin-induced pulmonary fibrosis in hamsters. Am. J. Pathol. 1983; 112(2):170–177. [PubMed: 6192723]
20. Anthony, ML.; Williams, NO.; Brindle, KM. Magnetic resonance methods of monitoring cell metabolism.. In: Jenkins, N., editor. Methods in Biotechnology, Vol 8: Animal Cell Biotechnology. Humana Press Inc.; Totowa, NJ: 1999.
21. Park JM, Park JH. Human in-vivo ^{31}P MR spectroscopy of benign and malignant breast tumors. Korean J. Radiol. 2001; 2(2):80–88. [PubMed: 11752975]
22. Pullinger B, Profka H, Ardenkjaer-Larsen JH, Kuzma NN, Kadlecek S, Rizi RR. Metabolism of [1-13C] pyruvate in the isolated perfused rat lung- an ischemia study. NMRBiomed. 2012; 25(10): 1113–1118.
23. Klier M, Schüler C, Halestrap AP, Sly WS, Deitmer JW, Becker HM. Transport activity of the high-affinity monocarboxylate transporter MCT2 is enhanced by extracellular carbonic anhydrase IV but not by intracellular carbonic anhydrase II. J. Biol. Chem. 2011; 286(31):27781–27791. [PubMed: 21680735]
24. Cobben NAM, Jacobs JA, van Dieijen-Visser MP, Mulder PGH, Wouters EFM, Drent M. Diagnostic value of BAL fluid cellular profile and enzymes in infections pulmonary disorders. Eur. Respir. J. 1999; 14(3):496–502. [PubMed: 10543266]
25. Drent M, Cobben NAM, Henderson RF, Wouters EFM, van Dieijen-Visser M. Usefulness of lactate dehydrogenase and its isoenzymes as indicators of lung damage or inflammation. Eur. Respir. J. 1996; 9:1736–1742. [PubMed: 8866602]
26. Johnson ML, Hussien R, Horning MA, Brooks GA. Transpulmonary pyruvate kinetics. Am. J. Physiol. 2011; 301(3):R769–R774.
27. Wimberger P, Ebner S, Marin-Grez M. Reduced glutathione inhibits rabbit and rat skeletal muscle lactate dehydrogenase and prevents dinitrophenol induced extracellular acidification by an epithelial cell line. Life Sci. 1997; 61(4):403–409. [PubMed: 9244366]
28. Rahman I, Adcock IM. Signaling and transcriptional regulation in inflammatory and immune cells: importance in lung biology and disease. Eur. Respir. J. 2006; 26(5):762–763.
29. Jones HA, Clark RJ, Rhodes CG, Schofield JB, Krausz T, Haslett C. *In vivo* measurement of neutrophil activity in experimental lung inflammation. Am. J. Respir. Crit. Care Med. 1994; 149:1635–1639. [PubMed: 7516252]
30. Jones HA, Schofield JB, Krausz T, Boobis AR, Haslett C. Pulmonary fibrosis correlates with duration of tissue neutrophil activation. Am. J. Respir. Crit. Care Med. 1998; 158:620–628. [PubMed: 9700143]
31. Beck WS. A kinetic analysis of the glycolytic rate and certain glycolytic enzymes in normal and leucemic leucocytes. J. Biol. Chem. 1955; 216:333–350. 15. [PubMed: 13252033]

32. Simon LM, Robin ED, Raffin T, Theodore J, Douglas WH. Bioenergetic pattern of isolated type II pneumocytes in air and during hypoxia. J. Clin. Invest. 1978; 61(5):1232–1239. [PubMed: 207732]
33. Rehn B, Bruch J, Zou T, Hobusch G. Recovery of rat alveolar macrophages by bronchoalveolar lavage under normal and activated conditions. Environ. Health Perspect. 1992; 97:11–16. [PubMed: 1396444]
34. Massaro GD, Gail DB, Massaro D. Lung oxygen consumption and mitochondria of alveolar epithelia and endothelial cells. J. Appl. Physiol. 1975; 38(4):588–592. [PubMed: 1141087]
35. Yoshii C, Nagata N, Tao Y, Suematsu R, Nikaido Y, Kido M. Relationship between inflammatory cells in bronchoalveolar lavage fluid and pathologic changes in the lung interstitium. Respiration. 1998; 65:386–392. [PubMed: 9782222]
36. Dik WA, McAnulty RJ, Versnel MA, Naber BAE, Zimmermann LJI, Laurent GJ, Mutsaers SE. Short course dexamethasone treatment following injury inhibits bleomycin induced fibrosis in rats. Thorax. 2003; 58:765–771. [PubMed: 12947134]
37. Zytemur ZA, Hacievliyagil SS, Iraz M, Samdanci E, Ozerol E, Kuku I, Nurkabulov Z, Yildiz K. Effects of iloprost on bleomycin-induced pulmonary fibrosis in rats compared with methyl-prednisolone. Rev. Port. Pneumol. 2012; 18(6):272–277. [PubMed: 22770817]
38. Bakowska J, Adamson IYR. Collagenase and gelatinase activities in bronchoalveolar lavage fluids during bleomycin-induced lung injury. J. Pathol. 1998; 185:319–323. [PubMed: 9771487]
39. Yi ES, Salgado M, Williams S, Kim S-J, Maslia E, Yin S, Ulich TR. Keratinocyte growth factor decreases pulmonary edema, transforming growth factor-beta and platelet-derived growth factor-BB expression, and alveolar type II cell loss in bleomycin-induced lung injury. Inflammation. 1998; 22(3):315–325. [PubMed: 9604718]
40. Li X, Zhang H, Soledad-Conrad V, Zhuang J, Uhal BD. Bleomycin-induced apoptosis of alveolar epithelial cells requires angiotensin synthesis de novo. Am. J. Physiol. Lung Physiol. 2003; 284(3):L501–L507.
41. Christensen PJ, Bailie MB, Goodman RE, O'Brien AD, Toews GB, Paine R III. Role of diminished epithelial GM-CSF in the pathogenesis of bleomycin-induced pulmonary fibrosis. Am. J. Physiol. Lung Cell. Mol. Physiol. 2000; 279:L487–L495. [PubMed: 10956623]
42. Drath DB, Harper A, Ghar J. The effect of tobacco smoke on the metabolism and function of rat alveolar macrophages. J. Cell Physiol. 1978; 95(1):105–113. [PubMed: 205549]
43. Simon LM, Robin ED, Raffin T, Theodore J, Douglas WH. Bioenergetic pattern of isolated type II pneymocytes in air and during hypoxia. J. Clin. Invest. 1978; 61(5):1232–1239. [PubMed: 207732]
44. Fisher AB, Furia L. Isolation and metabolism of granular pneumocytes from rat lungs. Lung. 1977; 154:155–165. [PubMed: 916725]
45. Ojima-Uchiyama A, Masuzawa Y, Sugiura T, Waku K, Saito H, Yui Y, Tomioka H. Phospholipid analysis of human eosinophils: high levels of alkylacylglycerophosphocholine (PAF) precursors. Lipids. 1988; 23(8):815–817. [PubMed: 3185116]
46. Dube DH, Bertozzi CR. Glycans in cancer and inflammation—potential for therapeutics and diagnostics. Nat. Rev. Drug Discov. 2005; 4(6):477–488. [PubMed: 15931257]
47. Jones HA, Cadwaller KA, White JF, Uddin M, Peters AM, Chilvers ER. Dissociation between respiratory burst activity and deoxyglucose uptake in human neutrophil granulocytes: implications for interpretation of ^{18}F-FDG PET images. J. Nucl. Med. 2002; 43(5):652–657. [PubMed: 11994530]
48. Sapey E, Stockley RA. COPD exacerbations. 2: Aetiology. Thorax. 2006; 61(3):250–258. [PubMed: 16517585]
49. Tanabe N, Muro S, Hirai T, Oguma T, Terada K, Marumo S, Kinose D, Ogawa E, Hoshino Y, Mishima M. Impact of exacerbations on emphysema progression in chronic obstructive pulmonary disease. Am. J. Respir. Crit. Care Med. 2011; 183:1653–1659. [PubMed: 21471102]
50. Fels AO, Cohn ZA. The alveolar macrophage. J .Appl. Physiol. 1986; 60:353–369. [PubMed: 3005225]
51. Niemeier RW. The isolated perfused lung. Environ. Health Perspect. 1984; 56:35–41.

52. Golman K, Zandt RI, Lerche M, Pehrson R, Ardenkjaer-Larsen JH. Metabolic imaging by hyperpolarized ^{13}C magnetic resonance imaging for *in vivo* tumor diagnosis. Cancer Res. 2006; 66(22):10855–10860. [PubMed: 17108122]

53. Devlin RB, McDonnell WF, Mann R, Becker S, House DE, Schreinemachers D, Koren HS. Exposure of humans to ambient levels of ozone for 6.6 hours causes cellular and biochemical changes in the lung. Am. J. Respir. Cell Mol. Biol. 1991; 4(1):72–81. [PubMed: 1846079]

54. Merezhinskaya N, Ogunwuyi SA, Mullick FG, Fishbein WN. Presence and localization of three lactic acid transporters (MCT1, –2, and –4) in separated human granulocytes, lymphocytes, and monocytes. J. Histochem. Cytochem. 2004; 52(11):1483–1493. [PubMed: 15505343]

55. Thind K, Chen A, Friesen-Waldner L, Ouriadov A Scholl TJ, Fox M, Wong E, Vandyk J, Hope A, Santyr G. Detection of radiation-induced lung injury using hyperpolarized (13)C magnetic resonance spectroscopy and imaging. Magn. Reson. Med. 2013; 70(3):601–609.

56. MacKenzie JD, Yen YF, Mayer D, Tropp JS, Hurd RE, Spielman DM. Detection of inflammatory arthritis by using hyperpolarized (13)C-pyruvate with MR imaging and spectroscopy. Radiology. 2011; 259(2):414–420. [PubMed: 21406626]

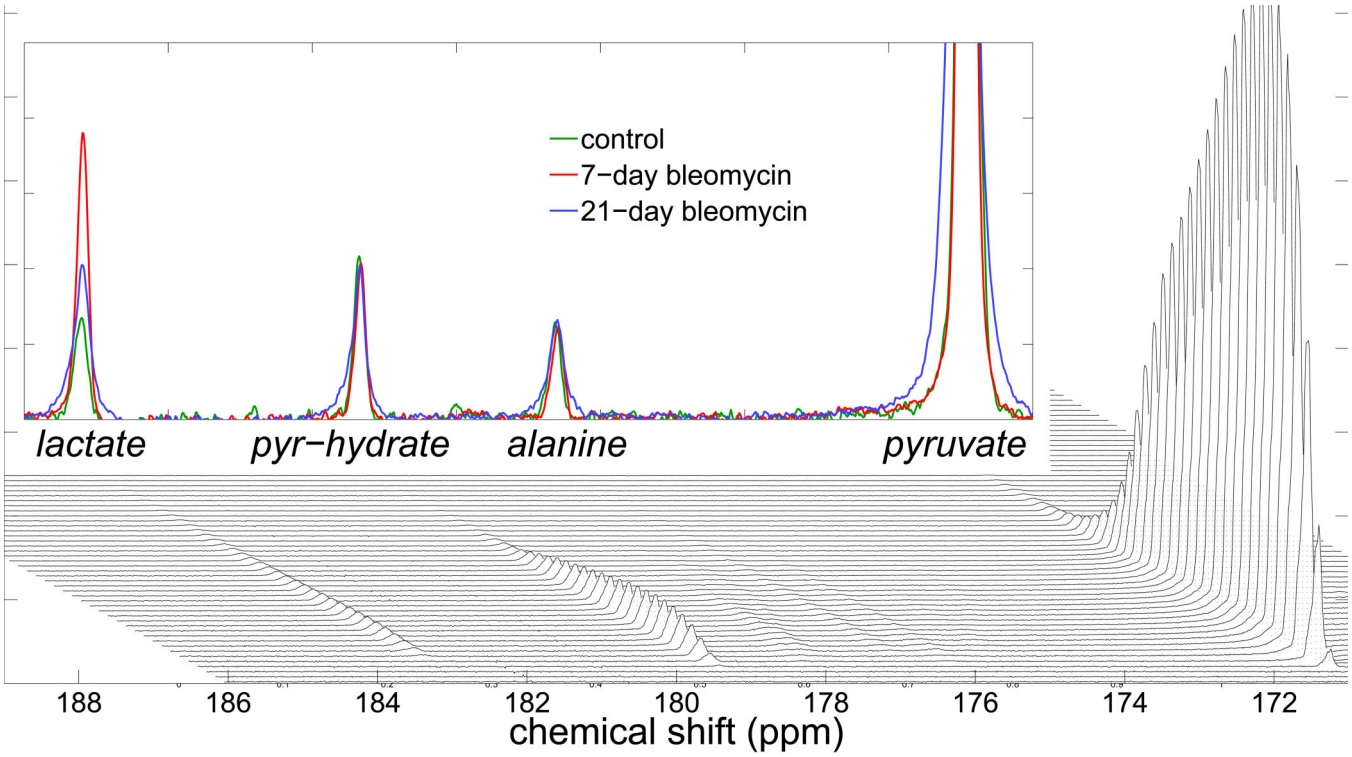

Figure 1.

A time-series of stacked ^{13}C spectra (bottom) show the immediate appearance of pyruvate and pyruvate-hydrate signal, followed by lactate and alanine. The unidentified peaks are impurities from the hyperpolarized pyruvate sample, and not indicative of biological activity. The time-evolution of signal levels is very similar between control and inflammatory groups, with the exception of the lactate signal, which is significantly increased in the diseased cohort. This can be seen in the three overlaid spectra, which are averages of the ten spectra between 20 and 30 seconds after the end of the hyperpolarized injection (top). The 7-day inflammatory model spectrum (red) is visually indistinguishable from the 21-day (blue) and control (green) spectra, except at the position of the lactate peak; at this position, the 21-day peak area exceeds that of the control by approximately a factor of two, and the 7-day exceeds the control by approximately a factor of three.

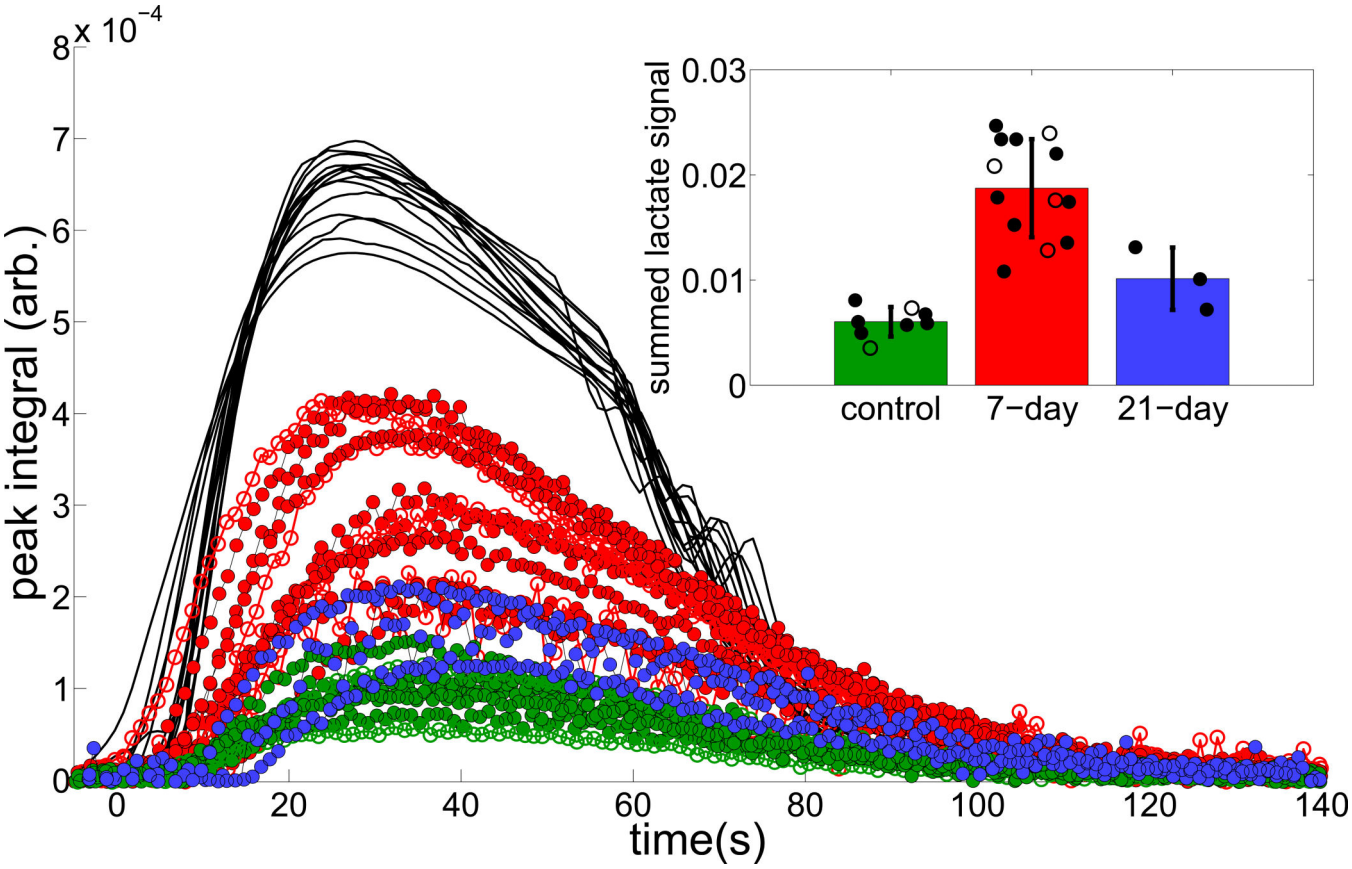

Figure 2.

Shows the full time-series of fit peak areas, in which the 7-day inflammatory group lactate peaks exceed those of the control group at all times, by an average factor of 3.3. Note that the signal amplitudes are scaled such that the sum of pyruvate areas $\Sigma p(t) = 1$, and times are shifted such that each injection is centered around $t = 50$. The inset bar graph shows the mean and average integrated lactate signal in the control (green), 7-day (red) and 21-day (blue) groups. In both plots, solid circles represent data acquired on the first ^{13}C injection and open circles represent data acquired on the second ^{13}C injection. When only first injections are considered, the 7-day group is statistically distinguishable from the other two groups ($p = 0.0003$). Although only six studies were repeated, no systematic change is evident (visually or by repeated measures ANOVA) between the groups due to the time delay between the two HP agent injections.

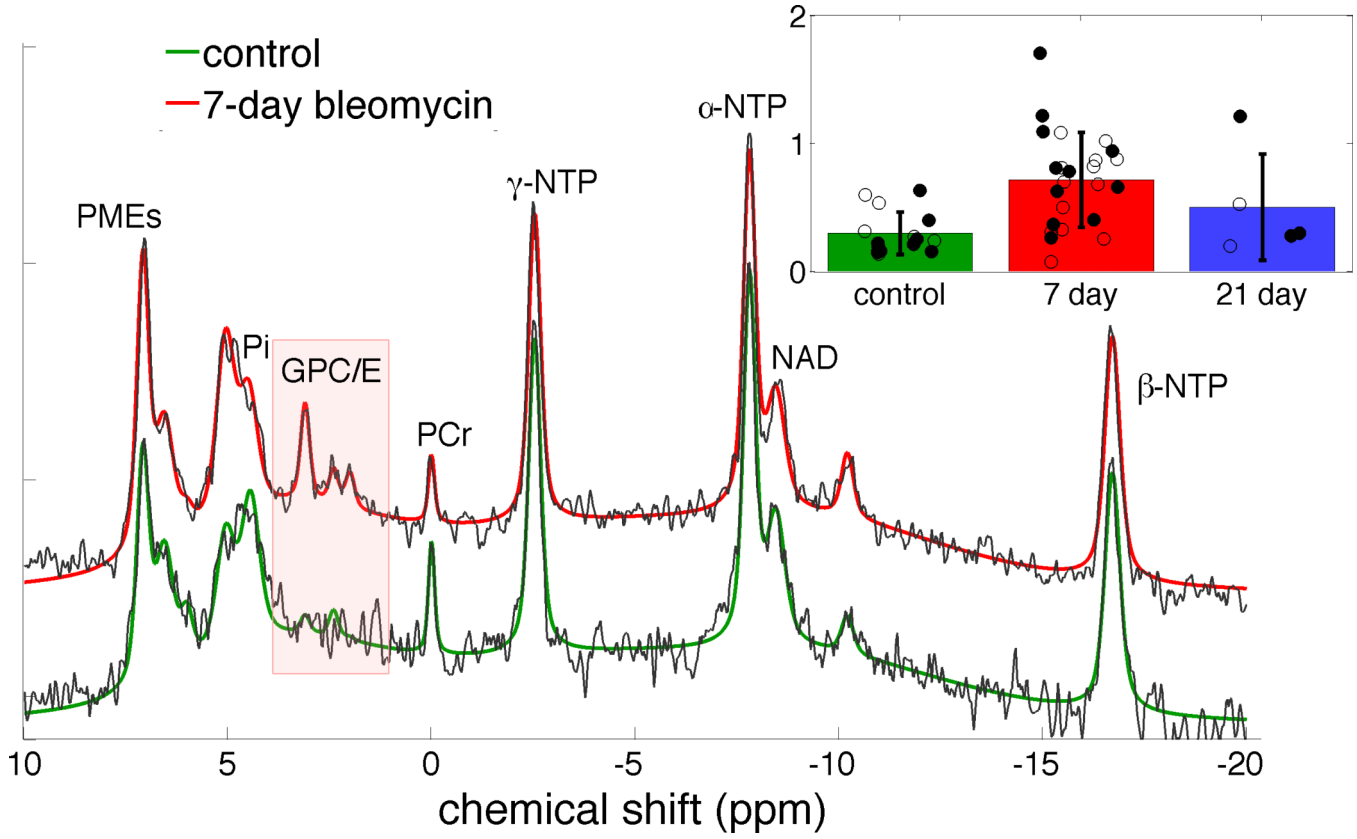

Figure 3.

a) Sample ^{31}P spectra from control (black with green fit), and 7-day (black with red fit) inflammatory model lungs show very similar patterns of high energy phosphates (NTP), inorganic phosphate (Pi), phosphomonoesters (PME) and phosphocreatine (PCr) but differ in a set of three peaks consistent with the known chemical shifts of the phosphodiesters glycerophosphocholine and glycerophosphoethanolamine (GPC/E) and, slightly upfield, phosphoglycans (PG). The figure inset shows a comparison of the three cohorts' summed GPC/E+GP fit peak areas. Cohort means and standard deviations are summarized by the corresponding black bars and individual GPC/E+GP peak areas appear as filled/open black circles for first/second injections.. Note that the individual peak areas are offset randomly in the horizontal direction for better visibility. Only the GPC/E/PG peaks differ between the groups; this difference is highly significant when comparing control and 7-day bleomycin groups ($p < 0.01$ whether all points or only first injections are compared). The 21-day group can not be distinguished from either of the other groups based on a t-test. All amplitudes are scaled to the corresponding Pi peak area.

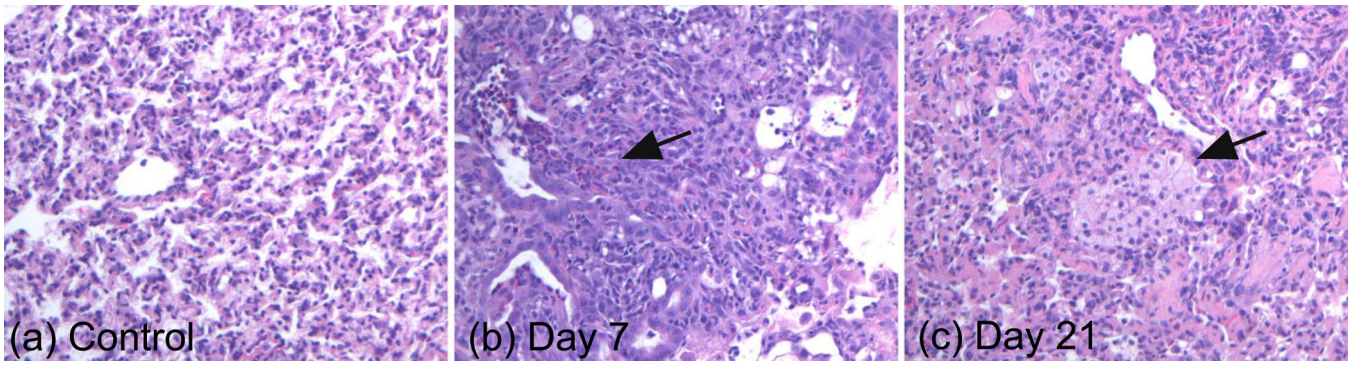

Figure 4.

Representative histological sections from control lung (a), 7-day post-bleomycin lung (b) and 21-day post-bleomycin lung (c). The sections were chosen to highlight the common characteristics of each group— in particular, the elevated neutrophils at 7 days and elevated macrophages at 21 days. A more objective evaluation of inflammatory cell density can be seen in **Table 1**. Note that the alveolar structure is somewhat distorted in all of the sections because the lungs were collapsed during the NMR studies and were not reinflated for histology.

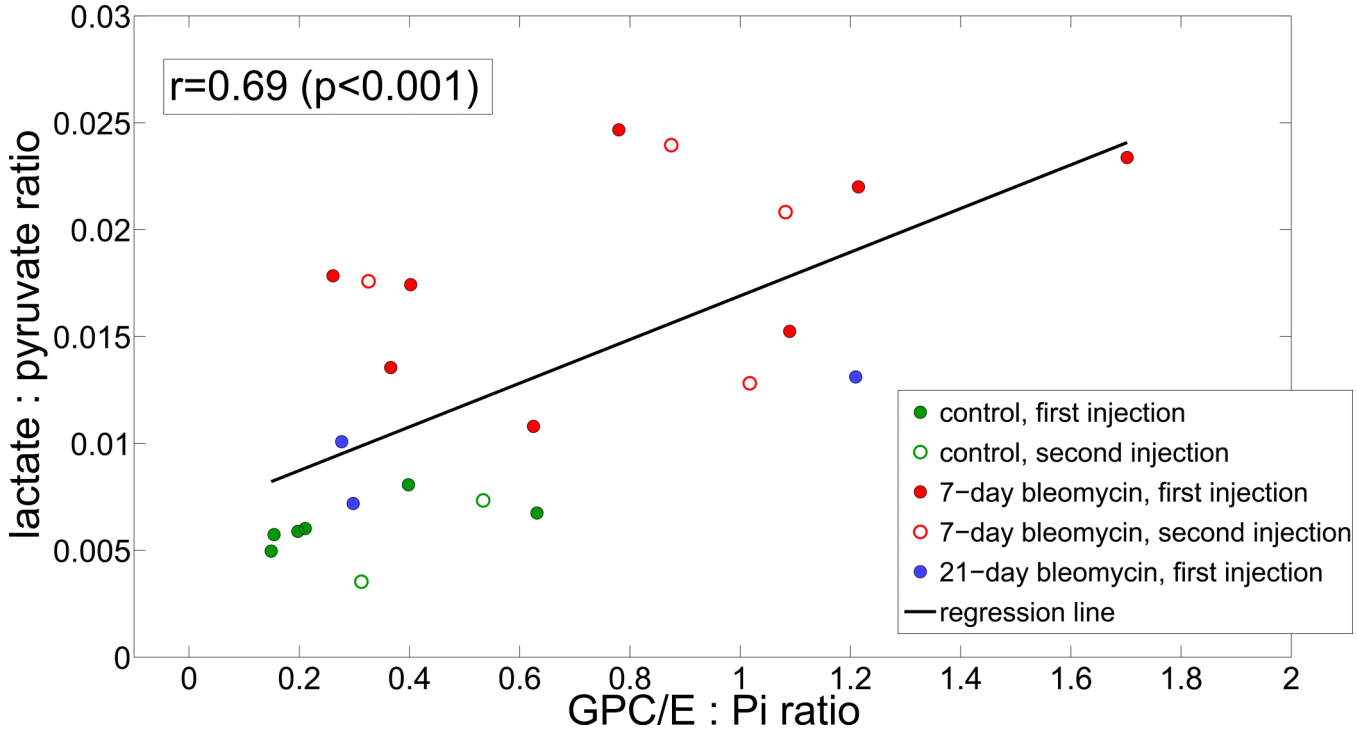

Figure 5.

Among all lungs, the increase in lactate produced by inflamed lungs is significant (approximately a factor of 3.3 at 7 days and a factor of 1.8 at 21 days) and correlates moderately well to the GPC/GPE peak increase observed using time-averaged ^{31}P spectroscopy of the lung. In the figure, the cohorts are distinguished as: control (green), 7-day (red) and 21-day (blue) cohorts. First and second injections in the same lung are distinguished as closed and open circles, respectively.

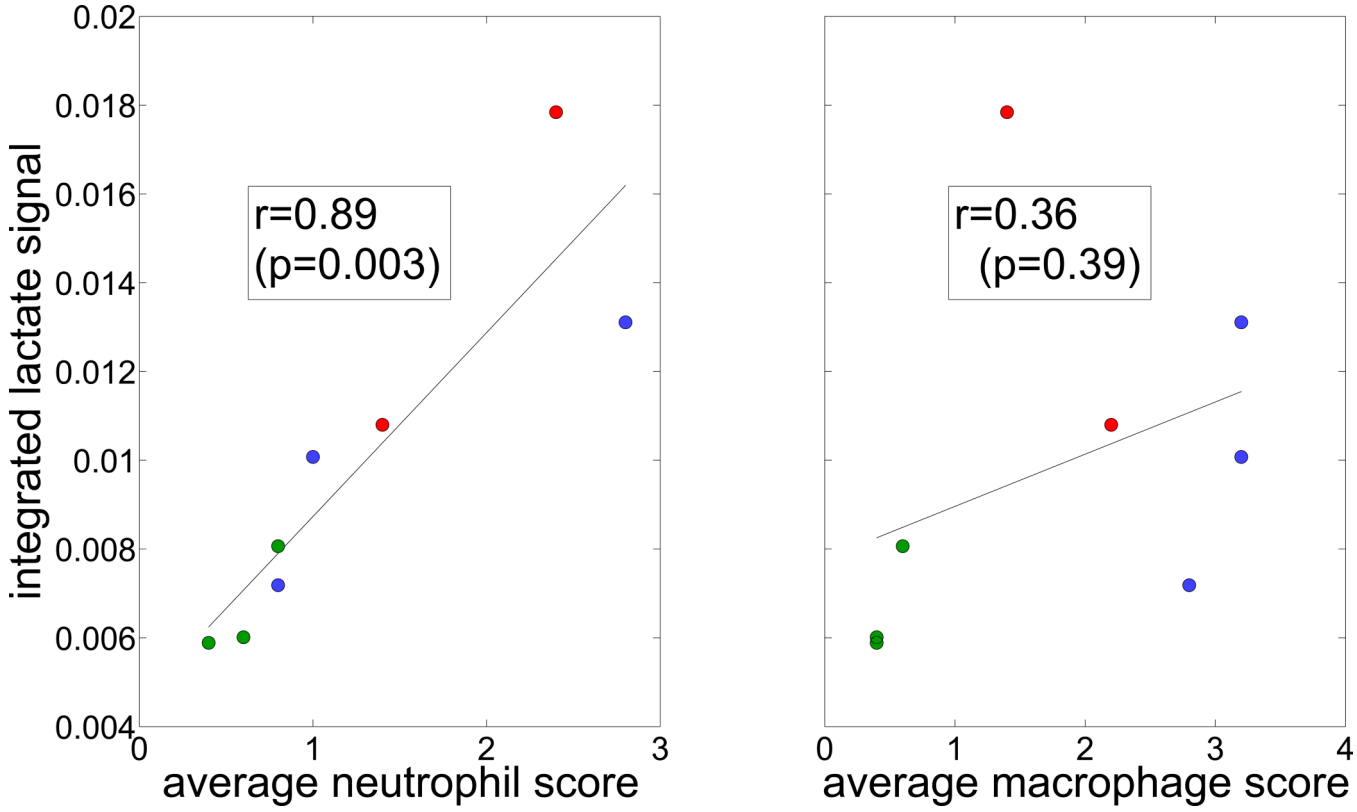

Figure 6.

Among all lungs for which histology was performed, the integrated lactate signal (normalized to integrated pyruvate signal) correlates well with the average neutrophil score as graded by a pulmonary pathologist. The correlation to the average macrophage score was not statistically significant. Scores were assigned from 0 (normal cell count) to 4 (severe and widely distributed inflammatory cells) based on a blinded, qualitative assessment of H&E sections five slices distributed throughout the lung.

Table 1

Average neutrophil, macrophage and lymphocyte score for each of the nine animals examined histologically.

	control	7-day	21-day
Average neutrophil score	0.6	2.7	1.0
	0.4	2.8	0.8
	0.8	1.4	2.8
Average macrophage score	0.4	1.4	3.2
	0.4	1.8	2.8
	0.6	2.2	3.2
Average lymphocyte score	0.4	0.6	1.2
	0.0	0.6	0.4
	0.0	1.0	0.4

Table 2

Summary Results of Analysis of Variance for Three Groups.

	Post Hoc Tukey HSD Test †			
Variables	**Cohorts**	**Mean Diff**	**95% CI***	***p***
^{13}C	7Day - Contol	0.0113	(0.006, 0.0167)	**0.0003**
	21Day - Contol	0.0039	(−0.003, 0.0107)	0.3226
	21Day - 7Day	−0.0074	(−0.014, −0.0008)	**0.0290**
^{31}P	7Day - Contol	0.4311	(0.1419, 0.7204)	**0.00250**
	21Day - Contol	−0.0001	(−0.4483, 0.4480)	0.98880
	21Day - 7Day	−0.4312	(−0.8603, −0.0022)	**0.04860**

*The numbers in the parenthesis shows the 95% confidence interval

†Post Hoc analysis was perfomed when ANOVA test was significant.